Measurement and Evaluation of Cloud free line of sight with Digital Whole Sky Imagers

Janet E. Shields*, Art R. Burden, Richard W. Johnson, Monette E. Karr, and Justin G. Baker

Marine Physical Lab, Scripps Institution of Oceanography, University of California San Diego, 9500 Gilman Dr., La Jolla CA 92093-0701

ABSTRACT

Cloud Free Line of Sight (CFLOS) statistics are important for evaluation of the impact of clouds on airborne and ground-based laser weapon scenarios. Whole Sky Imagers (WSI) have been developed at the Marine Physical Lab for many years, for several military applications including determining CFLOS and cloud persistence statistics. The Day/Night WSI systems are capable of acquiring data 24/7 for real-time monitoring of cloud conditions at test sites. Previously, CFLOS statistics based on earlier versions of the WSI were reported at BACIMO by MPL. More recently, sample data acquired for the DOE's ARM Program using the D/N WSI have been processed in order to extend these studies and especially to evaluate the behavior of CFLOS and persistence at low slant angles. Comparison of the results with the classic results by Lund and Shanklin are showing quite different behavior near the horizon, particularly in the presence of large nearly contiguous cloud fields. The data have also been sorted and analyzed as a function of cloud condition (cloud type and amount). We will present an overview of the WSI systems and the cloud algorithms used to identify the presence of clouds. The CFLOS statistics as a function of cloud type will be presented. Although a limited amount of D/N WSI data has been processed at this time, the results appear to be reasonable and significant. The WSI database spans many years at many sites, and is suitable for further evaluation of these initial results.

Key words: Whole Sky Imagers, cloud, cloud free line of sight, laser propagation, persistence, CFLOS, sky cover

1. INTRODUCTION

Cloud Free Line of Sight (CFLOS) statistics are useful for a number of military applications including missile defense (either airborne, ground based, or at sea), other laser applications such as laser communications, detection of visual and other targets through the atmosphere, modeling of cloud fields for scene simulators, and related applications. The Atmospheric Optics Group at Marine Physical Lab (MPL), Scripps Institution of Oceanography, University of California San Diego, has recently completed a study of CFLOS statistics, including Probability of CFLOS (PCFLOS), Probability of Cloudy Lines of Sight (PCLOS), and Persistence of CFLOS and CLOS. Recent results include PCFLOS as a function of cloud type.

These studies are based on ground-based the Day/Night Whole Sky Imager (D/N WSI)[1,2]. The WSI systems are automated digital imaging systems developed by the Atmospheric Optics Group. This recent study is based on a several months of data acquired every six minutes with a Day/Night WSI. The results are also supported by a more extensive analysis of Day WSI data taken in the 1980's[3,4]. A D/N WSI database consisting of several years of data at each of several sites is available for further studies.

CFLOS is defined simply as the probability that a given line of sight is cloud free, at a given point in time. For this study, we extracted CFLOS statistics as a function of zenith angle and cloud fraction, and as a function of cloud type. Persistence is defined as the probability that a line of sight will remain clear throughout an interval T, given that the line of sight is cloud free at time T_0. Persistence statistics were extracted as a function of zenith angle and of the cloud fraction at time T_0. Previous studies will be discussed in Section 2, and an overview of the WSI and its database will be

* jshields@ucsd.edu; phone (858) 534-1769; fax (858) 822-0665

discussed in Section 3. The results of this study will be discussed in the later sections. The results of the earlier study using the Day WSI were reported two years ago at BACIMO[2], and portions of this current study were reported earlier this year[5].

2. PREVIOUS STUDIES

The most extensive previous set of CFLOS and Persistence data that we are aware of is the data published by Lund and Shanklin[6,7,8]. The Lund data were acquired using a film camera, with infrared film and a fisheye lens, as well as a solar occultor to minimize stray light. Sample images are shown in Fig. 1. A template as shown in Fig. 2 was overlaid on each image, and a visual assessment of the presence of clouds in each circled point on the template was made and recorded.

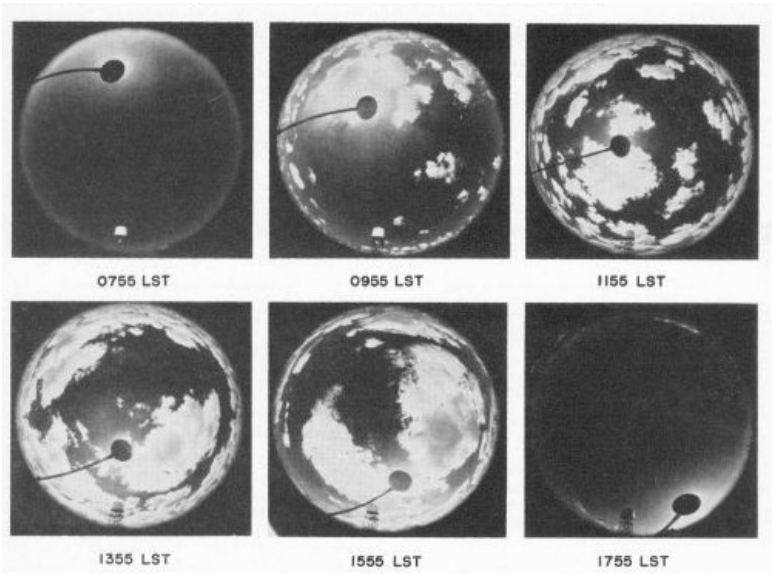

Figure 1. Sample raw images from Lund data set

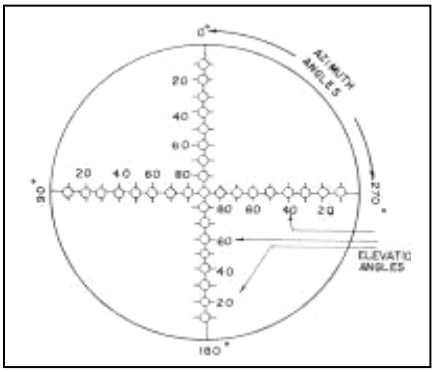

Figure 2. Template used to visually process Lund images

For the initial studies[6], hourly data taken in Columbia, Missouri for the summers of 1966 through 1969 were processed. Approximately 3300 images were processed and evaluated in each of 4 cardinal directions, to yield 13,000 observations of each zenith angle, or 110,000 observations total. The corresponding total cloud fraction was taken from the weather service ground-based records. The second Lund study[7] used data taken 3 times a day for a full three years. This data set included approximately 3100 images, and the results (for all cloud types combined) were nearly identical to the previous results. We have used these results in this paper.

The Lund data were identified using a human visual "image processor", which is normally a quite good cloud detector. However, human visual determination is not always consistent, and can be limited somewhat by the film characteristics. The Lund data has the disadvantage of limited data, representing only one site. The data also only go down to 80 degrees zenith angle. However, these data appear to have provided reasonable results for many years[9]. The Lund PCFLOS results for all cloud types are shown in Fig. 3.

As described in the Lund references, if PCFLOS as a function of cloud fraction and zenith angle is reasonably well known, then cloud fraction climatologies may be used to apply the results to multiple sites. In addition, if the data are sorted as a function of cloud type, then this information may be used to provide somewhat more accurate results. Although a thorough literature review is beyond the scope of this report, we would like to note that CFLOS modeling studies have been done, including modeling the results of Lund's study. Some current applications use the Lund data directly[9]. Examples of how to apply the data directly will be given in a later section.

3. THE DEVELOPMENT OF WSI SYSTEMS AT MPL

The original concept for the Whole Sky Imagers at MPL evolved out of the group's Atmospheric Optics program, a measurement and modeling program using multiple sensors for monitoring sky radiance, atmospheric scattering coefficient profiles, and other parameters related to vision through the atmosphere (Johnson et al 1980). The first automated WSI combined the features of the all-sky camera with the scanning radiometer systems that provided quantitative measurements of sky radiance distribution. Early systems were based on digital cameras with fisheye lenses, optical filter changers, relay optics to provide the proper image size and location, equatorial sun occultors to provide shading for the lens, and early versions of personal computers for automated control[3,4]. Fig. 4 shows some of this evolution. The film-based all-sky camera in use in a 1963 deployment is shown in Fig. 4a, and the automated Day-only WSI developed in the mid-1980's based on CID technology is shown in Fig. 4b.

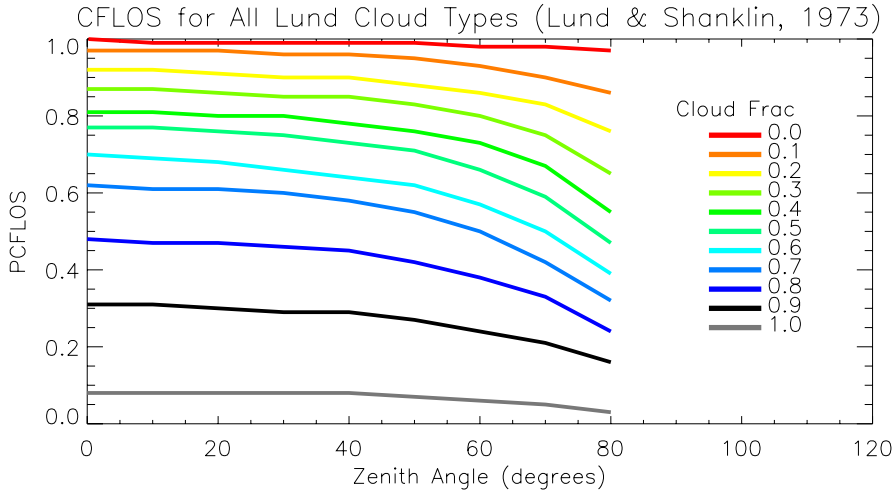

Figure 3. Lund PCFLOS for all cloud types

With the use of very low noise 16-bit CCD cameras and an occultor modified to handle both sun and moon, these systems were further developed into the Day/Night WSI shown in Fig. 4c[1,2]. Unlike the more common 24-bit color camera with 8-bit resolution in each color, this system has 16-bit (65,536 grey levels) in each spectral filter, as well as additional neutral density filters and exposure control for a useful dynamic range of over 10 logs or 10^{10}. As a result, the WSI data is fully onscale for 24/7, so that night sky between stars has an excellent signal to noise, yet bright clouds near the sun are also onscale. The system optics are fully shaded, providing outstanding data quality. Algorithm results can be extracted all the way down to the horizon, although these results are reported to an 88° zenith angle. Although more advanced WSI systems and other related systems have been recently developed at MPL[10,11,12], this study is based on data acquired with the version of the D/N WSI shown in Fig. 4c. Some typical images from the Day/Night WSI are shown in Fig. 5.

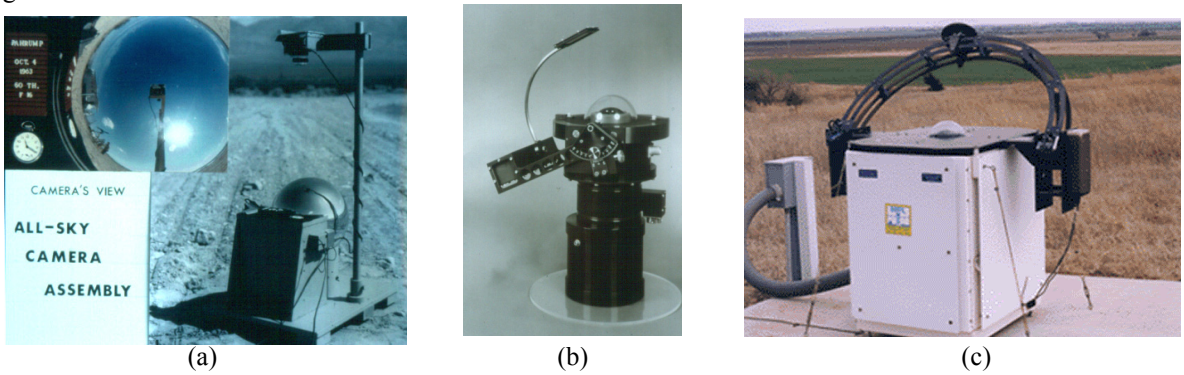

(a) (b) (c)

Figure 4: Some of the WSI Systems developed at MPL: a) the All-Sky Camera used in 1963; b) the Day-only digital WSI developed and used in the 1980's; c) the Day/Night WSI used since the early 1990's and used to acquire the data for this study.

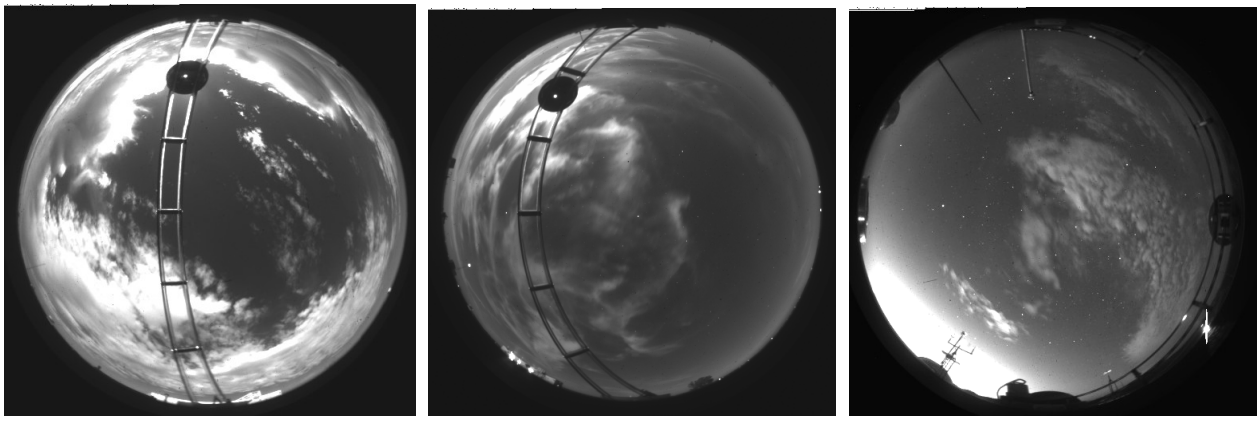

Figure 5: Sample imagery from the Day/Night WSI for sunlight, moonlight, and starlight conditions.

4. DATA EXTRACTION FOR THE CFLOS STUDY

Data has been acquired at multiple sites over many years under the auspices of the Department of Energy's Atmospheric Radiation Measurements (ARM) program[13]. We chose to base this study on data acquired at the Southern Great Plains (SGP) site in 2002. Approximately three million image sets are currently available in data archive for the D/N WSI. However, at the present time, the versions of the cloud algorithms used to process much of this data are not as accurate as desired for this study. As a result, data were processed using the MPL cloud algorithm. This cloud algorithm is based on the red/blue algorithm developed by MPL in the '80's[14,15] and more recently upgraded and improved. The algorithm is currently under further development; for example red skies at dawn often cause the current version of the algorithm to misidentify the sky (work is in progress to alleviate this problem). Any algorithm results that were not reasonable were eliminated from the study.

Sample algorithm results are shown in Fig. 6. Figures 6a and 6c show raw red images. Figures 6b and 6d show the cloud algorithm result, where white indicates optically opaque cloud, light blue indicates optically thin cloud, and darker blue indicates clear sky. Figures 6a and 6b show a case with multiple cloud layers, and Figures 6c and 6d show a case dominated by cirrus, possibly resulting from airplane contrails. More horizon pixels were masked for these two images than for most of the data in the set, because they are both from August, when it was necessary to mask out grasses that grew up into the field of view late in the summer.

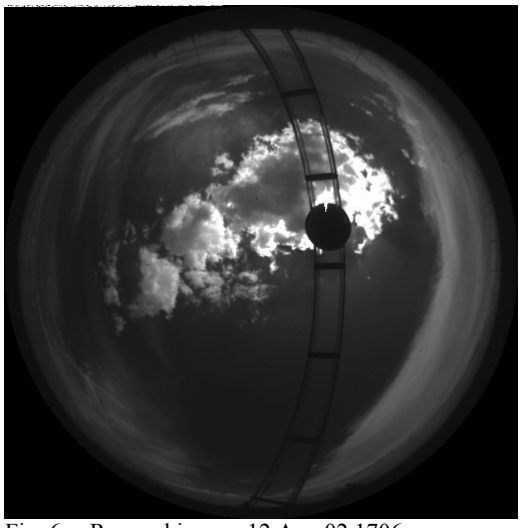

Fig. 6a. Raw red image, 12 Aug 02 1706z

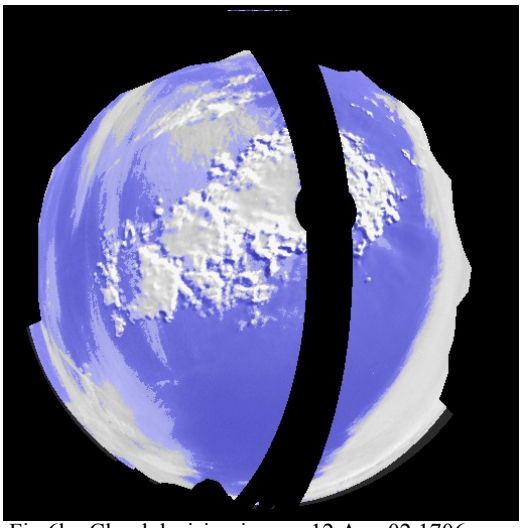

Fig 6b. Cloud decision image, 12 Aug 02 1706z

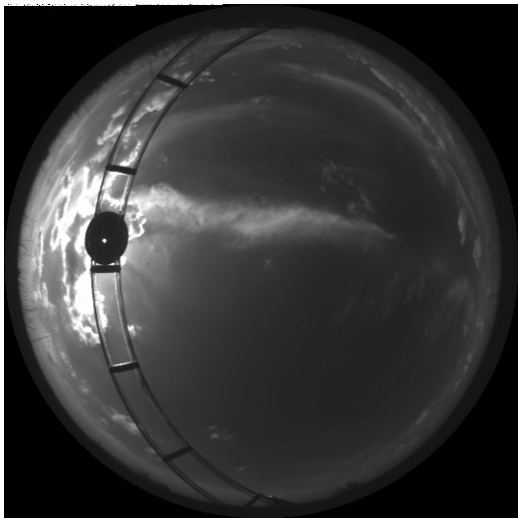

Fig. 6c. Raw red image, 16 Aug 02 2218z

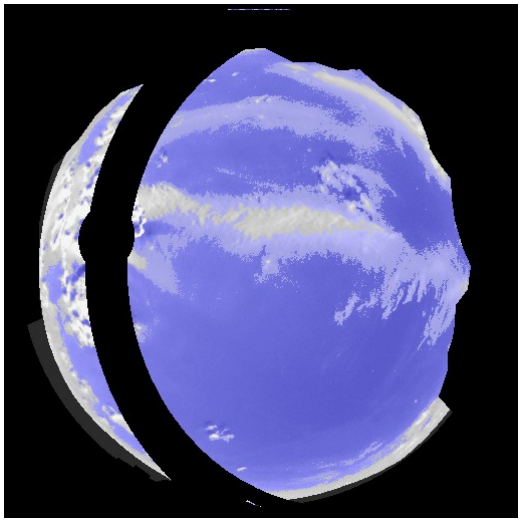

Fig 6b. Cloud decision image, 16 Aug 02 2218z

Figure 6. Sample Cloud Algorithm Results from this data set

Initially, this study used 3 months of data from the SGP site: February, March, and August '02. February and March are the cloudiest months, and August is the least cloudy month, based on the highest and lowest monthly mean of total sky cover. In the second part of the study, in which data were sorted as a function of cloud type, we found that there was insufficient data for certain combinations of cloud type and cloud amount. As a result, we sorted the weather reports to select additional days with the desired conditions, and supplemented the study with WSI data from these additional days. CFLOS determinations were extracted from the cloud decision images every 15 degrees in azimuth and 5 degrees in zenith angle up to 80 degrees, and every 1 degree from 81-90 degrees, as shown in Fig. 7. A total of 7081 images were processed, to extract about 170,000 points at each zenith angle, for a total of about 4,600,000 CFLOS data points. Lund lists the number of data points extracted at each zenith angle (except 0). These numbers are given, with the corresponding WSI data points, in Table 1. (The number of data points is slightly less near the horizon, where some points are blocked by the mask.)

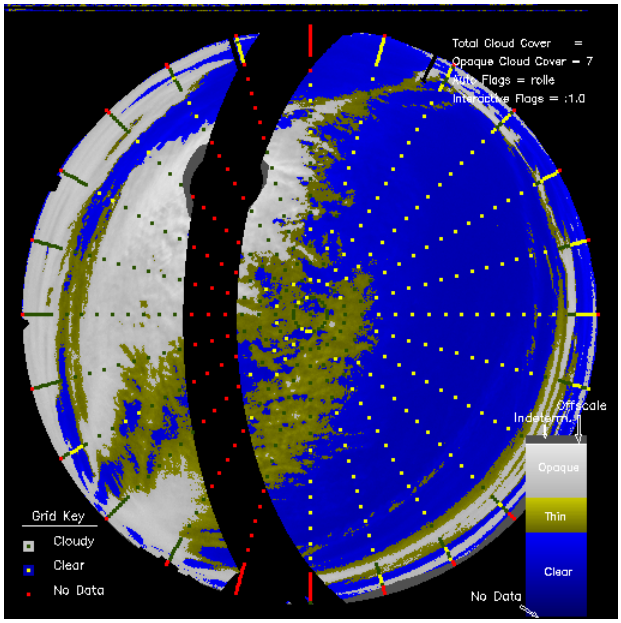

Figure 7. An illustration of the extracted CFLOS data points. In this illustration, thin cloud is colored dark yellow. Extracted data points are colored grey, white, and red, for cloud, clear, and no data respectively.

Table 1
Number of data points extracted at each zenith angle (except 0) as a function of cloud fraction

Cloud Fraction	WSI Study	Lund Study
0	31056	2276
.1	14688	568
.2	7728	576
.3	7248	800
.4	6624	450
.5	5784	356
.6	5808	548
.7	5832	544
.8	8376	664
.9	14976	788
1.0	61824	4760
Total	169944	12330

The data were further sorted for this study as a function of cloud form, using the Lund cloud categories cirriform, middle, cumuliform, and stratiform. We have also referred to the last two categories as low-level convective, and low-level non-convective. Like Lund, we used the numbers 1 – 4 to designate these cloud forms, and 5 to designate mixed cloud scenes. We also used 0 to designate the total of all cloud forms, and 6 to designate cases where the observer reported no cloud. Coincident hourly visual weather observations reported by site staff were used to determine appropriate cloud types for each image used in the study, while cloud fractions were obtained using the WSI daytime cloud algorithm. Each WSI image was examined to determine the validity of the hourly weather observations and identify off-hour cloud types

5. SAMPLE RESULTS OF THE CFLOS STUDY

The combined results for the full data set are shown in Fig. 8. In this figure, the PCFLOS results are shown as a function of zenith angle and cloud fraction. The zenith angle is 0 overhead, and 90 at the horizon. The cloud fraction is determined from the cloud decision images. Fig. 8 shows the results when both opaque and thin clouds are considered to block the line of sight. . The cloud fraction 0.0 category includes 0 – 5% cloud fraction. Similarly, the 1.0 category includes 95 – 100%. The other categories .1, .2, etc include cloud fractions 5% to 15%, 15% to 25%, etc. These results have also been slightly smoothed using a boxcar average.

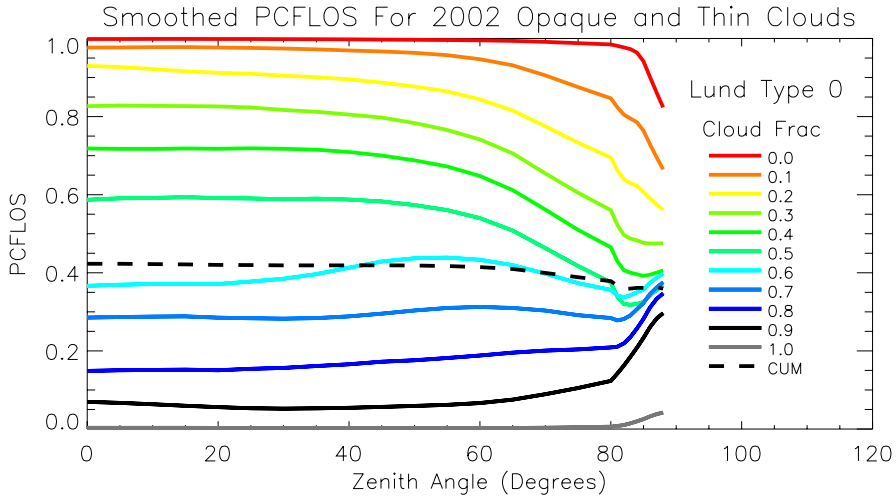

Figure 8. Probability of Cloud Free Line of Sight as a function of cloud fraction and zenith angle, including both opaque and thin clouds

For some applications, it may be that only opaque clouds need to be considered as blocking the line of sight. Fig. 9 shows a similar plot showing the PCFLOS for opaque clouds only. It is plotted as a function of TOTAL cloud fraction. As an example, note the curve for 0.9 cloud fraction. At the zenith, the probability of CFLOS is close to 0.1 if all clouds are considered, but goes up to about 0.3 if only opaque clouds are considered. In addition, the Probability for Cloudy Line of Sight for all cloud forms has been computed. A sample is shown in Fig. 10. This is simply the inverse of the PCFLOS plots.

The data in Fig. 8 may be compared with the Lund data in Fig. 3. We first note that the Lund curves are generally significantly higher at the zenith. For example, when the cloud fraction is 0.9 (black line), we would expect the PCFLOS to average to a value of about 0.1. The WSI data are near 0.1, however the Lund data are near 0.3. Similarly, when the cloud fraction is 0.6 (turquoise), the PCFLOS should be near 0.4, as it is in the WSI data, however in the Lund data it lies near 0.7. We believe this is due to an inconsistency between the observer values Lund used to provide cloud fraction, and the Lund CFLOS visually determined from the film. It is difficult to say whether the inconsistency in the Lund data is due to the CFLOS or the cloud fractions. Certainly the Lund data could be explained if the thin clouds were not observed or counted in the images (note how similar it is to Fig. 9). It could equally be explained if the ground observers overestimated cloud fraction. Because the WSI study uses the pixel-by-pixel determination of cloud presence to determine the cloud fraction from the imagery, it should be much more accurate. However, we should note that when

CFLOS statistics are used, it is important to be aware of whether the cloud fraction is determined from WSI or other ground-based sensors, from visual observers, or from satellite climatologies. That is, uncertainties in the site-specific cloud fraction statistics can affect the final conclusions. Further studies of WSI data taken at sites with trained observers should be considered to determine the WSI CFLOS statistics as a function of trained observer cloud fractions and satellite cloud fractions.

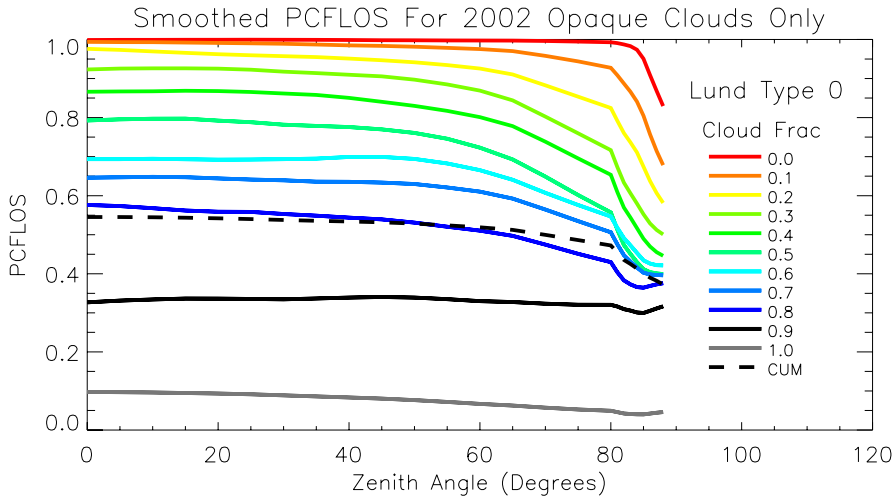

Figure 9. Probability of Cloud Free Line of Sight as a function of cloud fraction and zenith angle, including only opaque cloud regions

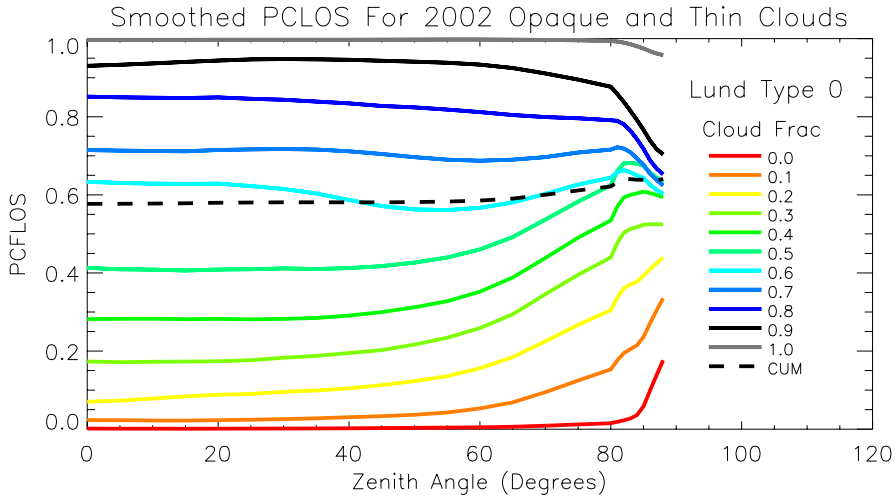

Figure 10. Probability of Cloudy Line of Sight as a function of cloud fraction and zenith angle, including opaque and thin clouds

Another very interesting difference between the Lund data in Fig. 3 and the WSI data I Fig. 8 is the behavior near the horizon. The Lund data consistently decrease as the horizon is approached. Under broken cloud conditions, the WSI PCFLOS data actually increase as the horizon is approached, and under scattered cloud conditions, the WSI PCFLOS data decrease much faster than the Lund data.

We believe this behavior is real and is a very significant finding. In the simple case of a broken cloud field of clouds with uniform distribution, limited horizontal extent, and significant vertical structure, we would expect the line of sight to be blocked more often at the horizon and PCFLOS to decrease toward the horizon under broken cloud conditions. However, in reviewing the images, we see far more clouds with more horizontal structure, or sheet-like behavior, than

we do clouds with vertical structure and small horizontal size. The clouds with more horizontal structure are primarily cirrus or stratus-type cloud layers. Under this cloud regime, it is reasonable that the CFLOS may increase at the horizon under broken cloud conditions.

We carefully evaluated the results for cloud fractions in the .8 category for one month, to determine whether the horizon behavior might be due to a weakness in the algorithm, but we found that in every case behavior at the horizon was real, and not an artifact of the algorithm. Time lapse series of the cloud motion at 6-min intervals gave us even more confidence in the algorithm results. Similarly, the clouds on the horizon under scattered cloud conditions do not appear to be caused by algorithm issues. Three typical examples are shown in Fig. 11.

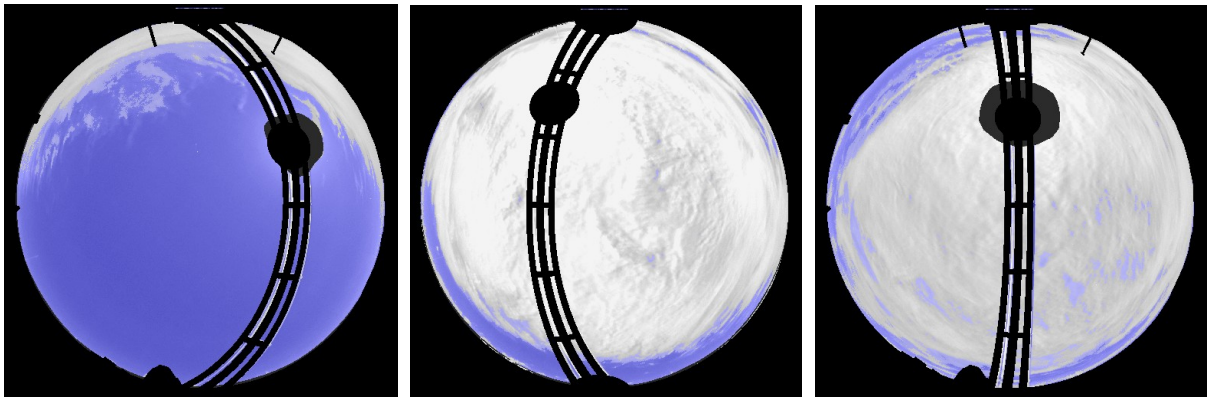

Fig. 11. Three samples of near-horizon algorithm behavior under scattered and broken conditions

The Lund data were all taken at a single site, Columbia MO. A large set of Day WSI data was acquired in the late 1980's (by MPL) at multiple sites, and is useful in evaluating whether this PCFLOS behavior as a function of zenith angle occurs at other sites. The set of processed Day WSI data is larger, however we don't have quite as much confidence in the results, as the data were acquired with a less accurate imaging system, and the algorithm was an earlier version. However, this data set has the advantage of multiple sites, as well as a large quantity of data. Over 95,000 image sets have been processed, and about 37 million data points were extracted for CFLOS studies. The processed data from this earlier data set was acquired at two sites in New Mexico, and sites in Montana, Florida, and Columbia Missouri. All sites except Columbia behaved like the Oklahoma D/N WSI data. For the Columbia data site, the opaque-only data behaved like Lund's and the opaque plus thin data behaved like the D/N WSI data. Sample results from the Day WSI are shown in Fig. 12.

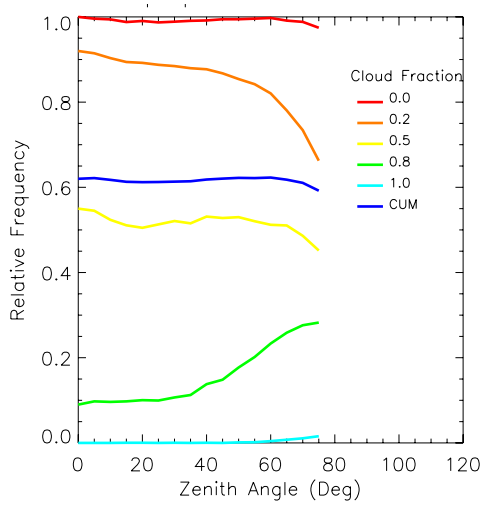

Fig. 12a. Day WSI PCFLOS for all clouds, 24,000 images, WSC Site

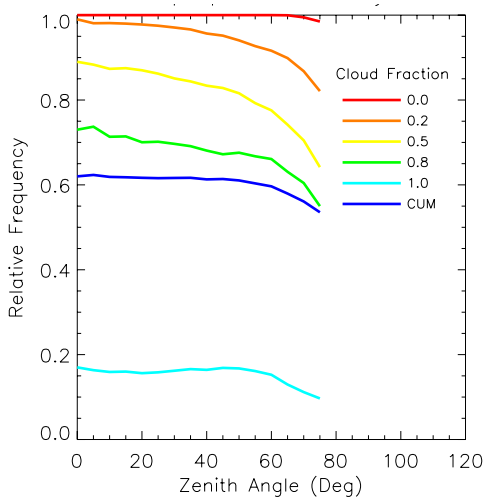

Fig. 12b. Day WSI PCFLOS for Opaque Only, 23,100 images, Columbia Missouri

For these reasons, we believe that the very different horizon behavior observed in the WSI data set is valid. There are many data years at other sites acquired with the D/N WSI, and as we improve the algorithm, we hope to further investigate this data in order to further evaluate this horizon behavior and the conditions under which it occurs.

The sorted data as a function of cloud category are shown in Figure 13. As might be expected, the absolute magnitudes of the curves do not change significantly, however the shape at the horizon changes significantly, depending on whether the cloud category is dominated by clouds of large horizontal extent.

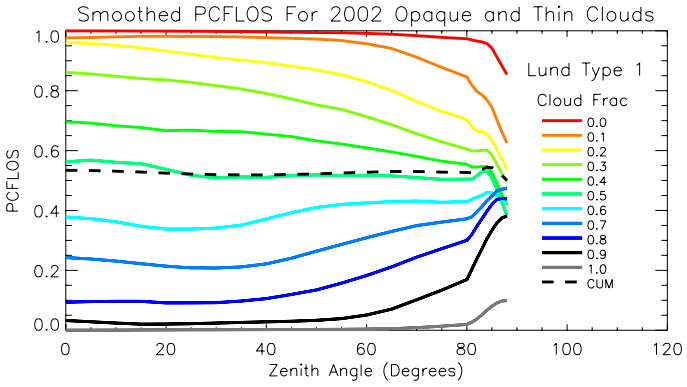

Fig. 13a. Cirroform or high clouds

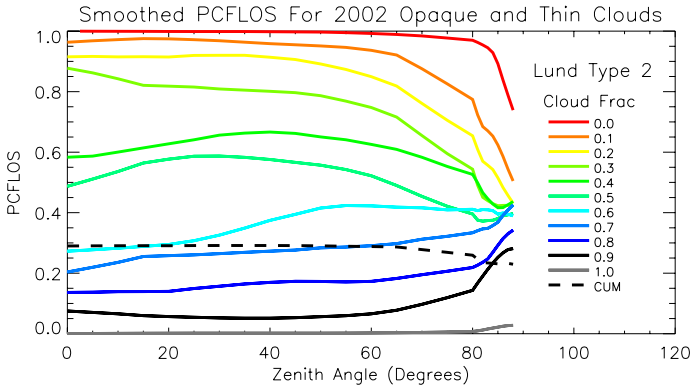

Fig. 13b. Middle clouds, such as Alto-cumulus

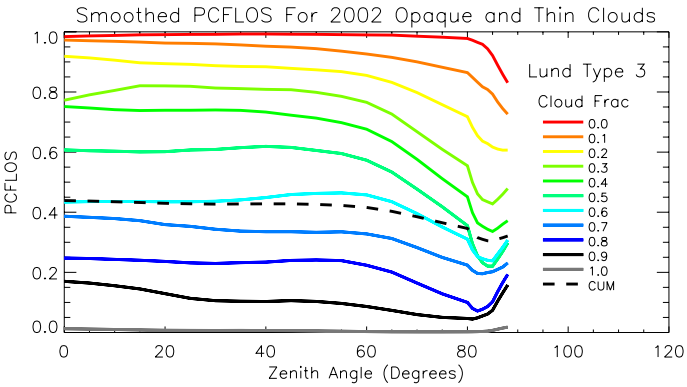

Fig. 13c. Cumuliform, or low convective clouds

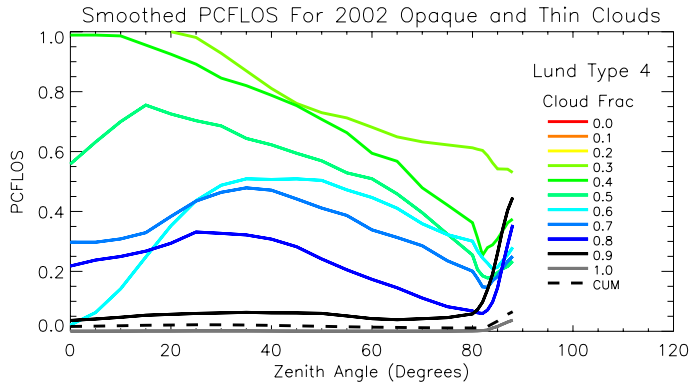

Fig. 13d. Stratiform, or low non-convective clouds

In Figure 13, most of the data samples (i.e. combination of cloud category and cloud fraction) included 1000 or more data points. However, in the case of the low non-convective clouds, there were 0 cases with cloud fraction 0, .1, and .2, and there were less than 100 for several other cloud fractions. As a result, the type 4 data from this study should generally not be used.

6. APPLICATION OF THE PCFLOS DATA

To determine PCFLOS for a random site in a random direction, we use Method A of Lund & Shanklin (1973). This method uses the matrix of PCFLOS values as a function of zenith angle and cloud fraction (**C** matrix), and a site-dependent vector of relative frequency of cloud fraction for a site (**K** vector), to obtain a PCFLOS vector as a function of zenith angle for the given site. The equation is given below.

$$ {}_{\alpha}P_1^A = {}_{\alpha}C_s K_1 $$

where ${}_{\alpha}\mathbf{P}_1^{\,A}$ is a column vector of α rows, one row for each angle considered; ${}_{\alpha}\mathbf{C}_s$ is a matrix of α rows and s columns each, one row for each zenith angle, one column for each sky cover category; and $\mathbf{K}_1$ corresponds with a column of s rows. For example, Table 2 provides a matrix of PCFLOS as a function of cloud fraction and elevation angle (**C** matrix).

The **C** matrix for the full database is shown in Table 2. In Table 3, we have provided several examples of the $\mathbf{K}_1^N$ vector: Lund's example for all cloud forms for Columbia, MO; the statistics for Feb/Mar 02 and for Aug 02 at SGP; and the statistics based on clear, scattered, broken, and overcast for Baghdad from the ISMCS data base*. The results are shown for several zenith angles in Table 4.

Table 2
C Matrix consisting of PCFLOS Results, all cloud forms, opaque and thin clouds

	Sky Cover (tenths)										
Zen Ang (deg)	0	1	2	3	4	5	6	7	8	9	10
0	1.00	0.98	0.93	0.83	0.72	0.59	0.37	0.29	0.15	0.07	0.00
10	1.00	0.98	0.92	0.83	0.72	0.59	0.37	0.29	0.15	0.06	0.00
20	1.00	0.98	0.91	0.83	0.72	0.59	0.37	0.29	0.15	0.06	0.00
30	1.00	0.97	0.90	0.82	0.72	0.59	0.38	0.28	0.16	0.05	0.00
40	1.00	0.97	0.90	0.81	0.71	0.59	0.41	0.29	0.17	0.05	0.00
50	1.00	0.96	0.88	0.78	0.69	0.57	0.44	0.30	0.18	0.06	0.00
60	1.00	0.95	0.84	0.74	0.65	0.54	0.43	0.31	0.19	0.07	0.00
70	0.99	0.91	0.78	0.65	0.56	0.46	0.40	0.30	0.20	0.09	0.00
80	0.98	0.85	0.70	0.56	0.47	0.38	0.36	0.28	0.21	0.12	0.01
81	0.98	0.82	0.66	0.52	0.43	0.34	0.34	0.28	0.21	0.14	0.01
82	0.98	0.81	0.64	0.50	0.41	0.32	0.34	0.28	0.22	0.16	0.01
83	0.97	0.80	0.63	0.49	0.40	0.32	0.34	0.29	0.24	0.18	0.01
84	0.96	0.79	0.62	0.48	0.40	0.32	0.35	0.31	0.26	0.21	0.02
85	0.94	0.76	0.61	0.48	0.39	0.33	0.36	0.32	0.28	0.23	0.03
86	0.90	0.73	0.59	0.48	0.40	0.34	0.37	0.35	0.31	0.26	0.03
87	0.86	0.70	0.58	0.48	0.40	0.36	0.39	0.36	0.33	0.28	0.04
88	0.82	0.66	0.56	0.48	0.41	0.37	0.40	0.38	0.35	0.30	0.04

Table 3
K Matrix for Several Locations, consisting of probability of cloud fraction

Cloud Fraction	Lund Columbia Summer	WSI SGP Feb-Mar	WSI SGP Aug	ISMCS Baghdad Jan	ISMCS Baghdad Jun
0.0	0.187	.196	.292	.298	.878
0.1	0.047	.075	.094	.062	.022
0.2	0.047	.033	.038	.062	.022
0.3	0.049	.026	.041	.062	.022
0.4	0.037	.017	.024	.062	.022
0.5	0.031	.019	.023	.061	.013
0.6	0.045	.022	.028	.060	.004
0.7	0.045	.023	.032	.060	.004
0.8	0.055	.043	.045	.060	.004
0.9	0.065	.085	.074	.060	.004
1.0	0.392	.462	.310	.134	.002

In Table 4, the CFLOS probabilities for the SGP site are higher for August than for Feb/Mar, as expected. The results for Baghdad are significantly higher, particularly for the June period. The column for Lund is lower than Lund reported; it uses the Lund K vector, but the WSI C matrix, which is more consistent than the Lund data, as noted earlier. As noted above, we have also derived information similar to that shown in Table 2 as a function of cloud form, and also derived similar results for the most and least cloudy months. At sites where probabilities of cloud fraction as a function of cloud form are known, this information can be used to further improve the accuracy of the results. At other sites, where this probability distribution is not known, it is reasonable to use the least and most cloudy C matrices, as well as the matrix for whatever cloud type is dominant, to determine expected ranges of results.

* The International Station Meteorological Climate Summary Ver 4.0 (ISMCS) provides this information for 2600 worldwide sites. The database may be obtained on CD-ROM from the National Climatic Data Center online store. The web address for the product is http://ols.nndc.noaa.gov/plolstore/plsql/olstore.prodspecific?prodnum=C00268-CDR-A0001

Table 4
Resulting PCFLOS for specific sites and zenith angles

Zenith Angle	Lund Columbia Summer	WSI SGP Feb-Mar	WSI SGP Aug	ISMCS Baghdad Jan	ISMCS Baghdad Jun
0	0.40	0.37	0.52	0.60	0.97
20	0.40	0.37	0.51	0.60	0.96
40	0.40	0.37	0.51	0.60	0.96
60	0.40	0.37	0.51	0.59	0.96
80	0.36	0.35	0.48	0.53	0.93
88	0.35	0.33	0.43	0.49	0.78

7. SAMPLE PERSISTENCE RESULTS

For many applications, it is important to know how long a CFLOS condition is apt to persist. By persistence, we mean that given that there is a CFLOS in a given direction at time 0, what is the probability that it will remain clear throughout the interval T. The D/N WSI data were taken at 6-minute intervals. Using the earlier Day WSI data, taken at 1 min intervals, we did a study to determine how much error results if data are acquired only at 5-minute intervals and used to estimate persistence based on 1-min intervals. The error was reasonably small. For example, for one hour, the persistence probability for the tested site was 0.74 based on 1-minute intervals, and 0.78 based on 5-minute intervals. Therefore we felt it reasonable to use this 6-minute data to evaluate persistence, although it should be recognized that the results may be a few percentage points high.

Persistence results were computed for February, March, and August of 2002. Sample persistence results are shown for March in Figures 14 and 15. Fig. 14 shows the persistence as a function of look angle. Fig. 15 shows the persistence for a specific look angle, as a function of cloud fraction at time 0. Results should not be used beyond approximately 4 hours, because the data beyond 4 hours became too sparse to be representative of the general case beyond this interval.

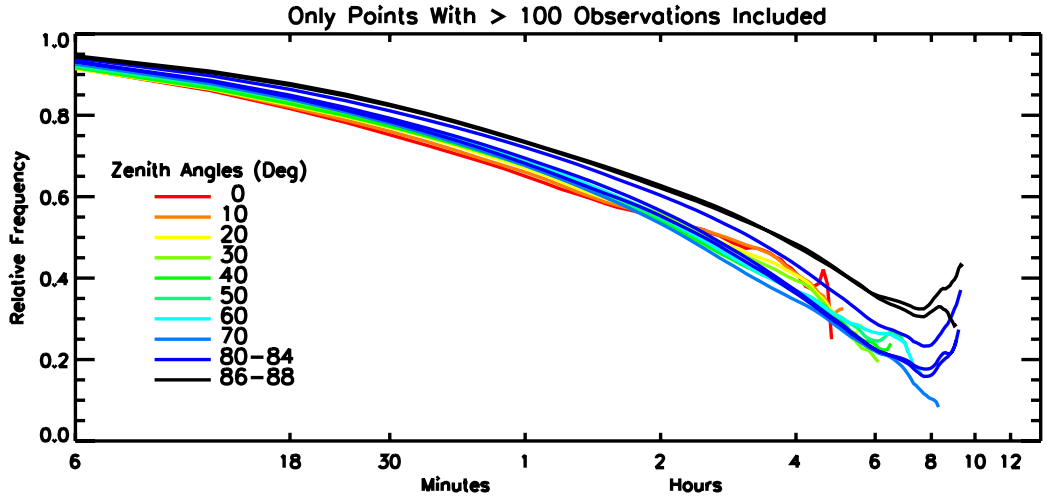

Figure 14. Persistence for CFLOS including both opaque and thin clouds

Fig. 14 shows that the persistence is, on average, quite high. Even after 3 hours, we have a probability of about 50% or more at all angles. However, near the zenith, the persistence depends strongly on initial conditions, as shown in Fig. 15. Fig. 15 shows the persistence as a function of both look angle and initial conditions. Near the horizon (plot on the right), the persistence is quite good under all conditions, including relatively clear (red, orange) and relatively cloudy (blue). But overhead (left plot of Fig. 15), the persistence is only good if the sky is initially reasonably clear (red, orange

curves). This is in large part due to perspective; evaluation indicates it is not an artifact of algorithm issues. The computed persistence tables may be used in conjunction with cloud climatologies from specific sites to estimate the overall persistence probabilities, in a manner similar to that illustrated in Section 6.

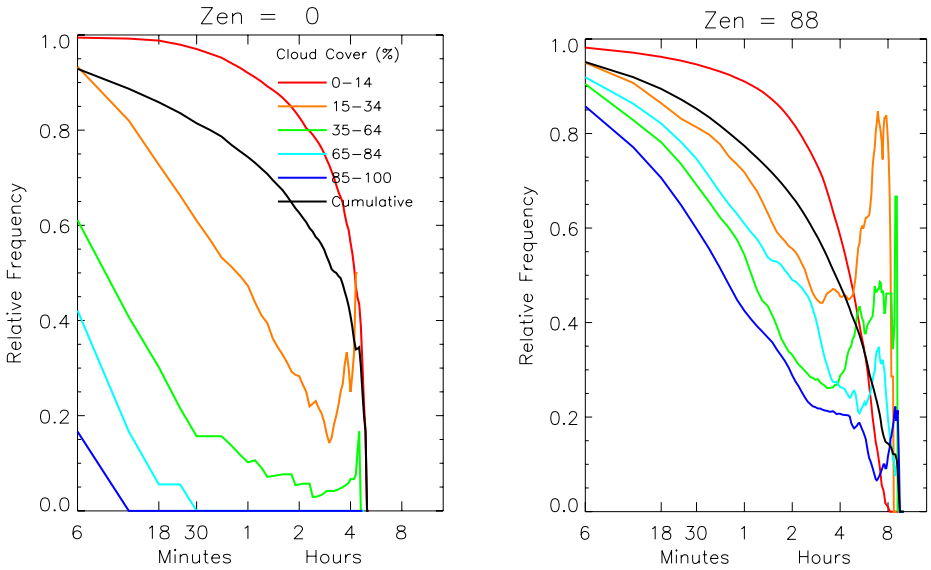

Fig. 15. Persistence for the Zenith and the Near-Horiz

8. SUMMARY

The Day/Night Whole Sky Imager has been used to acquire many years of data at many sites. Data from several months has been processed to extract Cloud Free Line of Sight and Persistence statistics. The results show that the CFLOS probabilities are somewhat lower than shown in the Lund data set. They also show that PCFLOS rises toward the horizon in broken cloud conditions, and falls more sharply than predicted by Lund in scattered cloud conditions. Detailed analysis of the processed images reveals that this does not appear to be an artifact of the data processing, but can be expected for regions with frequent contiguous or sheet-like clouds. The persistence results show that persistence probabilities for PCFLOS are typically quite high, with about a 50% probability for periods of 3 hours. The persistence results also depend very strongly on initial conditions, i.e., the cloud fraction at the start of the interval. Persistence probabilities can be quite low when significant clouds are present. We feel these results are reliable, as they are based on a substantial data set of over 7000 images was used, and the cloud algorithm results were quite good all the way down to the horizon. These data can also be used to provide a variety of mission-specific statistics. The WSI archive includes more than 3 million image sets taken at many sites over many years, and these data may be used for further evaluation of CFLOS and Persistence for a variety of applications.

9. ACKNOWLEDGEMENTS

We would like to express our appreciation to Jerry Bukley and the Boeing SVS in Albuquerque, New Mexico, for their contributions to this effort. Thanks to Ann Slavin and the Air Force Starfire Optical Range for supporting the algorithm development, as well as an earlier CFLOS analysis that contributed to this effort. And finally, we appreciate DOE's Atmospheric Radiance Measurements program for supporting the fielding of the D/N WSIs used in this study, and for kindly providing the data to us.

10. REFERENCES

1. J. E. Shields, R. W. Johnson, M. E. Karr, and J. L. Wertz, *Automated Day/Night Whole Sky Imagers for Field Assessment of Cloud Cover Distributions and Radiance Distributions*, Tenth Symposium on Meteorological Observations and Instrumentation, American Meteorological Society, 1998.

2. J. E. Shields, R. W. Johnson, M. E. Karr, A. R. Burden, and J. G. Baker, *Whole Sky Imagers for Real-time Cloud Assessment, Cloud Free Line of Sight Determinations and Potential Tactical Applications*, The Battlespace Atmospheric and Cloud Impacts on Military Operations (BACIMO) Conference, Monterey, CA. http://www.nrlmry.navy.mil/bacimo.html, 2003.

3. R. W. Johnson, W. S. Hering, and J. E. Shields, *Automated Visibility and Cloud Cover Measurements with a Solid State Imaging System*, University of California, San Diego, Scripps Institution of Oceanography, Marine Physical Laboratory, SIO 89-7, GL-TR-89-0061, NTIS No. ADA216906, 1989.

4. J. E. Shields, R. W. Johnson, and T. L. Koehler, *Automated Whole Sky Imaging Systems for Cloud Field Assessment*, Fourth Symposium on Global Change Studies, American Meteorological Society, 1993.

5. J. E. Shields, A. R. Burden, R. W. Johnson, M. E. Karr, and J. G. Baker*, New cloud free line of sight statistics measured with digital Whole Sky Imagers*, International Symposium on Optical Science and Technology, SPIE the International Society for Optical Engineering, August 2005.

6. I. Lund, and M. D. Shanklin, *Photogrammetrically Determined Cloud-Free Lines-Of-Sight Through The Atmosphere*, Journal of Applied Meteorology, August 1972.

7. I. Lund, and M. D. Shanklin, *Universal Methods for Estimating Probabilities of Cloud-Free Lines-Of-Sight Through The Atmosphere*, Journal of Applied Meteorology, February 1973.

8. I. Lund, *Persistence and Recurrence Probabilities of Cloud-Free and Cloudy Lines-of-Sight Through the Atmosphere*, Journal of Applied Meteorology, October 1973.

9. D. Nahrstedt, *Cloud Modeling for Laser Weapon Propagation Analysis*, in Laser Weapons Technology, Proceedings of the SPIE, Vol.4034. Edited by T. Steiner and P. Merritt. 24 - 25 April 2000. Pp. 69- 81.

10. J. E. Shields, R. W. Johnson, M. E. Karr, A. R. Burden, and J. G. Baker, *Daylight Visible/NIR Whole Sky Imagers for Cloud and Radiance Monitoring in Support of UV Research Programs*, International Symposium on Optical Science and Technology, SPIE the International Society for Optical Engineering, 2003.

11. U. Feister, J. Shields, M. Karr, R. Johnson, and M. Woldt, *Ground-based Cloud Images and Sky Radiances in the Visible and Near Infrared Region from Whole Sky Imager Measurements*, EUMP31, EUMETSAT Satellite Application Facility Workshop, Dresden Germany, 20-22 November 2000, 79-88, 2000.

12. J. E. Shields, R. W. Johnson, M. E. Karr, A. R. Burden, and J. G. Baker, *Calibrated Fisheye Imaging Systems for Determination of Cloud Top Radiances from a UAV*, International Symposium on Optical Science and Technology, SPIE the International Society for Optical Engineering, 2003.

13. J. E. Shields, M. E. Karr, T. P. Tooman, D. H. Sowle, and S. T. Moore, *The Whole Sky Imager – A Year of Progress*, Proceedings of the Eighth Atmospheric Radiation Measurement (ARM) Science Team Meeting, 1998.

14. R. W. Johnson, T. L. Koehler, and J. E. Shields, *A Multi-Station Set of Whole Sky Imagers and A Preliminary Assessment of the Emerging Data Base*, Proc. Of the Cloud Impacts on DOD Operations and Systems, 1988 Workshop pp. 159 – 162 1988.

15. T. L. Koehler, R. W. Johnson and J. E. Shields, *Status of the Whole Sky Imager Database, Proceedings of the Cloud Impacts on DOD Operations and Systems*, 1991 Conference, 1991.